Novel Rapid Shutdown Strategies or Runaway Electron Suppression in DIII-D

N. Commaux 1), L.R. Baylor 1), N.W. Eidietis 2), T.E. Evans 2), E.M. Hollmann 3), D.A. Humphreys 2), V.A. Izzo 3), A.N. James 3), T.C. Jernigan 1), P.B. Parks 2), J.C. Wesley 2) and J.H. Yu 3)

1) Oak Ridge National Laboratory, Oak Ridge, Tennessee, USA
2) General Atomics, P. O. Box 85608, San Diego, California 92186-5608, USA
3) University of California San Diego, La Jolla, California, USA

E-mail contact of main author: commaux@fusion.gat.com

Abstract. New rapid shutdown strategies have been recently tested in the DIII-D tokamak to mitigate the runaway electrons (RE). Disruptions in ITER are predicted to generate multi-MeV REs that could damage the machine. Thus the mitigation of REs is critical for the reliability of ITER. These tests included new methods to mitigate the REs generation processes, methods to allow a harmless deconfinement of the REs and feedback control of the position of the RE beam to prevent interaction with the vacuum vessel. The RE generation process in ITER is expected to be mainly an avalanche process which can be mitigated at high-density levels n_{crit} by collisional drag. To reach this density, new particle injection schemes have been developed on DIII-D. The multi-valve massive gas injection (MGI), the shattered pellet injection and the shell pellet injection. The experimental results show an improvement of the penetration of the particles injected with the SPI compared to MGI. Other strategies have been also developed to harmlessly deconfine REs. The main method tested was applying a non-axisymmetric magnetic perturbation in order to disturb the RE confinement. This method enabled to deconfine the seed RE population before the avalanche process could amplify the RE beam. The last method tested was to use the poloidal coils system of DIII-D to control the position of the RE beam and prevent it from contacting the wall. This method proved effective in preventing high current RE beam from touching the wall and providing more time to apply other mitigation techniques to an existing RE beam.

1. Introduction

Prevention and mitigation of the harmful effects from disruptions are essential to reliable operation of ITER. One of the potentially most harmful effects from a disruption is the generation of runaway electrons (RE). These high energy (10s of MeV) focused electron beams can damage elements of the first wall if they strike and penetrate the material surfaces. Thus new rapid shutdown strategies have been recently tested in the DIII-D tokamak to mitigate RE. These strategies use different mechanisms to mitigate the RE. One of the most commonly tested is to collisionally drag the RE by increasing the density up to n_{crit} [1]. To increase the density, the "usual" method known as massive gas injection (MGI) is to inject a significant amount of gas (several 100 Pa.m^3 in DIII-D) through fast valves. In addition two new techniques were developed and tested recently on DIII-D: the shattered pellet injection (SPI) and the shell pellet injection (SHPI). These techniques were tested on lower single null edge localized mode (ELM)ing H mode plasmas. The second strategy tested is to control the position of an existing RE beam to prevent contacts of the high current RE beam with the vacuum vessel first wall. The last strategy tested on DIII-D is to use resonant magnetic perturbation (RMP) to lower the confinement of the RE to prevent the formation of a significant RE beam. This technique was applied on DIII-D by using in vessel coils in order to generate a non-axisymmetric magnetic field on plasmas prone to generate significant amounts of RE. RMP and feedback control were tested on DIII-D on discharges producing reliably significant RE population by using symmetric, limited, low elongation (κ=1.3-1.4) target plasmas terminated by an argon pellet, so the runaway beam naturally forms near the mid-plane. These RE beams had an amplitude in the 100-600 kA range and an average energy of ~20 MeV [2].

2. Collisional Suppression

In order to obtain a collisional suppression of RE, the total electron density must increase up to levels close to n_{crit}. This value is estimated using a 0D calculation of the toroidal electric field generated during the current quench (CQ) by the plasma current decay. In the fastest plasma current decay cases in DIII-D, this value is estimated at ~5×10^{22} m^{-3}. To do so, three techniques were tested on DIII-D: MGI, SPI and SHPI.

2.1 Massive Gas Injection

The massive gas injection (MGI) consists in injecting massive quantities of gas through fast valves. This method has been tested on DIII-D using the six fast-valves array MEDUSA [3]. A modified version of the original MEDUSA I injector has been used to conduct a systematic injected gas quantity (Q) and target plasma thermal energy variation experiment with helium MGI. This modified MEDUSA II injector was modified in order to implement the new SPI injector at the same location. Thus this injector feeds the gas through a 1.3 m long coaxial duct supporting the SPI breaker plate described in Sec. 2.2. This study enabled primarily to observe that the implementation of this restricted duct in front of the MEDUSA injector had a strong effect on the assimilation fraction $f_{assim} = N_{He}^{2+}/N_{He} = N_e/2N_{He}$ of the MGI system, N_e, N_{He} and N_{He}^{2+} being the total in-plasma free electron number, the total injected He number and the corresponding in-plasma fully-ionized He number. f_{assim} dropped from ~0.3 with MEDUSA I down to ~0.1 for MEDUSA II. The phenomenon that could explain this difference is the lower gas conductance of the annular duct forcing the gas pulse from MEDUSA to become wider in time. This explanation is supported by the results of the Q scans with constant plasma conditions. Figure 1 summarizes the results of this scan. There are two ways Q can be changed: by increasing the valve pulse duration or by changing the number of valves injecting simultaneously. Both were tested and Fig. 1 shows that the behavior changes dramatically according to the way Q is increased. Figure 1(a) shows that with a short 1 ms pulse duration, increasing Q (30–130 $Pa.m^3$) by increasing the number of valves operated, the assimilation fraction remains constant since N_e increases linearly with the number of valves thus Q. On the contrary Fig. 1(b) shows that with a fixed number of valves, increasing Q by increasing the pulse duration is not as efficient: N_e appears to saturate for a pulse duration above 1.5–2 ms. It appears that in the Q range tested here, the assimilation fraction is not directly dependent on Q but on the duration of the injection. This critical time of 1.5–2 ms appears to be correlated with the time delay between the time the gas pressure front hits the plasma and the time of the TQ onset [4]. This could be interpreted as the fact that the plasma can assimilate and ionize the gas for as long as there is significant thermal energy available in the plasma since this energy is lost rapidly after the TQ onset. To test directly the influence of the thermal energy content, a thermal energy scan was thus achieved on DIII-D by changing the neutral beam input power from 0 (ohmic) to 15 MW and injecting a constant helium Q (330 $Pa.m^3$ of helium with the same number of valves and pulse duration). The results of this thermal energy scan are shown on Fig. 2. This figure shows that the thermal energy has clearly an effect for weak injected power (up to 5 MW) thus weak thermal energy content with a strong increase of f_{assim}. Beyond this value, f_{assim} saturates at ~0.09. This saturation could be due to the fact that the favorable higher thermal energy content is compensated by

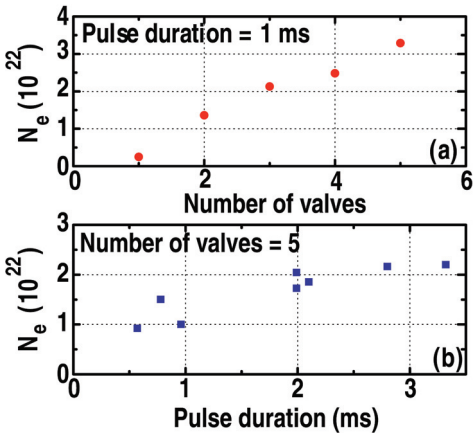

FIG. 1. MEDUSA-II gas quantity and plasma thermal energy variation experiments.

the possible stronger MHD activity triggering a faster loss of the plasma energy thus reducing the time available to assimilate the injected particles. These data show that MGI efficiency relies on fast delivery of the particles linked with a short valve pulse duration and a high conductivity of the gas duct. It shows also that the thermal energy content can improve this fraction up to a certain limit probably linked with MHD activity.

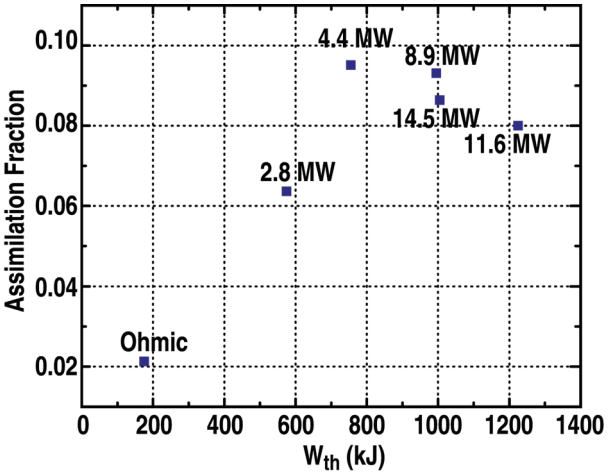

FIG. 2. Assimilation fraction as a function of the thermal energy content of the discharge.

2.2 Shattered Pellet Injection

The SPI technique consists of the injection of a large cryogenic pellet (15 mm x 20 mm on DIII-D). Before entering the plasma, the pellet is shattered into submillimeter fragments by impacting on two metal breaker plates. Shattering the pellet increases surface area for a more efficient ablation (according to preliminary 1D calculations) and protects the first wall from possible damage by impact from an intact pellet. The DIII-D SPI system injects enough particles into the plasma to reach an average electron density close to n_{crit} [5]. Experiments were carried out using the SPI technique to terminate successfully six discharges. The plasma conditions in these discharges were a toroidal field of 2.1 T, plasma current of 1.5 MA and neutral beam injection power of 013.4 MW. The pellets injected in these discharges were deuterium pellets injected with a speed range of 500–600 m/s and containing ~1.9×10^{23} atoms (400 Pa.m^3). Local densities were determined using the visible bremsstrahlung emission of the plasma measured with several visible spectrometers. These measurements taken at different toroidal locations enabled a lower bound estimate (because of signal saturation) of the total number of electrons N_{tot} in the discharge during the disruption. A typical example of the time evolution of N_{tot} during a SPI induced fast shutdown is shown in Fig. 3. This figure shows first that the maximum N_{tot} value is ~4.5×10^{22} electrons, which indicates a 24% assimilation fraction during this SPI induced shutdown. This assimilation fraction appears to increase weakly with the thermal energy content of the discharge for the neutral beam injection (NBI) heated discharges (the assimilation fraction varying between 18% and 24% for thermal energy content varying between 172 and 1660 kJ). The ohmic case seems to be an exception: the assimilation process appears to be longer thus improving the assimilation when compared to a weakly heated discharge. Figure 3 shows also that N_{tot} varies significantly during the fast shutdown: it decays very fast during the thermal quench (TQ), but starts to increase again after the onset of the CQ. The fast decrease during the TQ can be explained by the cooling of the plasma lowering the ionization rate, but not why it increases at the

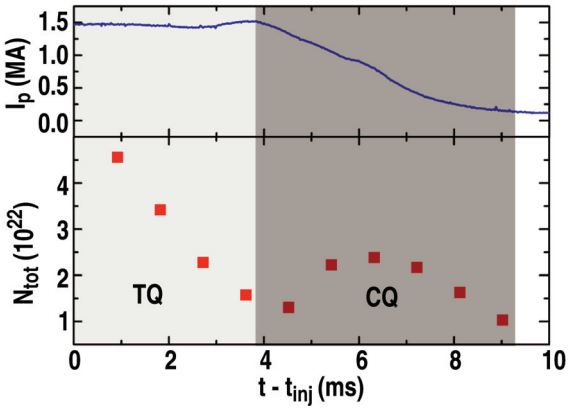

FIG. 3. Plasma current (upper) and N_{tot} (lower) during an SPI induced shutdown with thermal energy content of 1600 kJ (t_{inj} being the injection time). The light shaded area shows the TQ phase and the dark shaded one the CQ phase.

beginning of the CQ. Since the heating power is rather constant during this phase, the fact that N_{tot} increases could indicate an improvement of the particle confinement at the beginning of the CQ possibly due to a re-healing of the magnetic surfaces destroyed during the TQ MHD activity. The experiments carried out recently on DIII-D provided also for the first time a direct comparison between the MGI (using the MEDUSA II configuration since the MEDUSA I was not available anymore) and SPI techniques using the same plasma target, the same injected species and the same amount of particles. Figure 4 shows the line-integrated density during an ohmic plasma rapid shutdown using comparable MGI and SPI (400 Pa.m^3 of D_2 in both cases applied on the same plasma scenario). Since the central interferometry chord is located at a toroidal location 150 degrees apart from the injection location, this density measurement shows the particles that have already been transported and homogenized in the plasma. The maximum line integral density in the SPI case is twice as high as the maximum MGI density. The assimilation fraction is thus ~15% for MGI compared to ~25% for the SPI. The timing of the homogenization process is also more favorable for SPI. The SPI reaches the maximum density when the plasma current is 80% of its initial value. The MGI case reaches its maximum density when the plasma current is down 40% of the initial current. The fact that MEDUSA II was used for these tests has to be taken into account though. It is possible that the results would have been closer using the more optimal MEDUSA I configuration. This faster rise of the density for the SPI all around the torus may improve the efficiency of the collisional mitigation since the avalanche process depends on the absolute value of the plasma current as well as on the toroidal electric field. This faster rise of the density could indicate different transport mechanisms. The SPI would rely on parallel transport in the core plasma since it appears to penetrate much deeper than MGI that stays at the edge as colder and slower neutrals then mix with the plasma due to MHD events during the CQ [6].

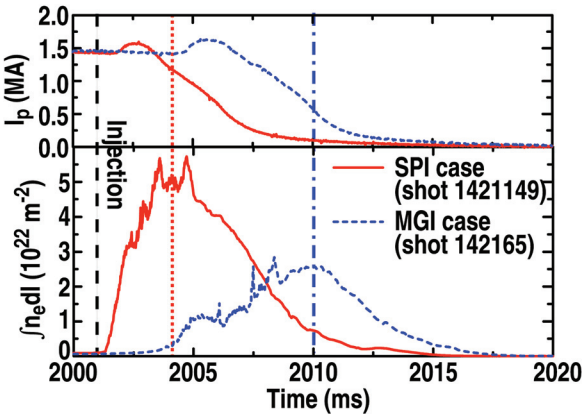

FIG. 4. Line-integrated density during SPI (solid) and MGI (dashed) rapid shutdown of an ohmic plasmas. The vertical lines show the time when the density starts to roll-over for the SPI (dot) and MGI (dash-dot).

2.3 Shell Pellet Injection

The SHPI basic principle is to fire a pellet consisting of a hard shell and dispersive payload at the plasma. The hard shell ablates away as the pellet transits through the plasma edge. Upon reaching the plasma core, the shell breaks open, releasing the dispersive payload throughout the core region. Two different types of dispersive payloads have been proposed: dust grains or high-pressure gas. Proof-of-principle shell pellet experiments were conducted in DIII-D using small (outer diameter ~2 mm, thickness ~0.4 mm) polystyrene shells filled with either pressurized (10 bar) argon gas or with boron powder. The pellets were fired at an initial velocity $v \approx 350$ m/s at the plasma core. These small shell pellets did not disrupt the plasma, but penetrated in to normalized minor radius $r/a \approx 0.5$ before burning through and releasing their payload. The payload release, ionization, and rapid (within about 10 ms) dispersion through the core were observed in visible camera imaging, with charge-exchange recombination, and with UV spectroscopy. Following the successful demonstration of the shell pellet concept with small shell pellets, large shell pellet experiments were attempted in

2009. In these experiments, large (outer diameter ≈ 1 cm, wall thickness ≈ 0.4 mm) polystyrene shells filled with boron powder were fired at velocity $v \approx 200$ m/s through the plasma core. These large shell pellets did shut down the discharge and initiate the TQ but did not break open in the plasma. Figure 5 shows a pellet radial trajectory and shell wall burn through of a large and small shell pellet. Pellet trajectory and burn through are both estimated from fast camera data — the trajectory by assuming the out-of-plane position is close to the vacuum trajectory (confirmed by center stack strike marks in the case of the large shell pellets); and the burn through by assuming that pellet ablation rate is proportional to ablation plume brightness, with a normalization of mass ablated obtained using total observed electron density rise from interferometers. Figure 5(a) shows the large shell pellet trajectory — the pellet can be seen to initiate the TQ upon crossing the $q=2$ surface.

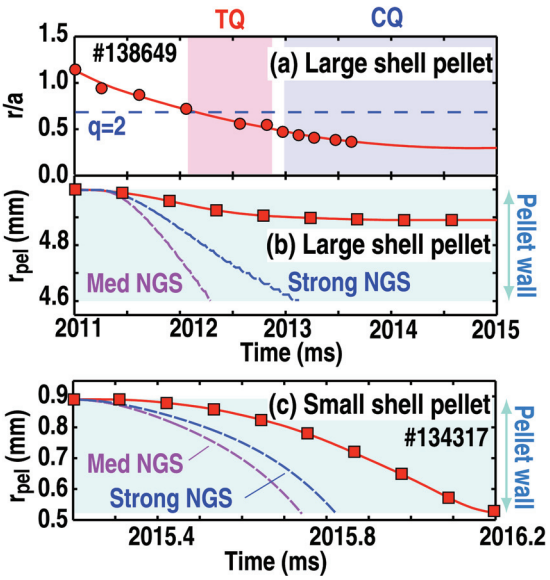

FIG. 5. (a) Pellet trajectories r/a as a function of time for a large shell pellet. Experimental (solid) and calculated (dash) pellet burnthrough of a large (b) and small (c) shell as a function of time.

The curve in Fig. 5(a) is due to the pellet trajectory missing the plasma magnetic axis. Figure 5(b) shows burn through of the pellet walls as a function of time for a large shell pellet. From this figure, it is apparent that the large shell pellet wall is estimated to have ablated about one-fourth of the way through. After $t \approx 2013$ ms (end of the TQ), ablation effectively turns off and the large shell pellet passes through the rest of the plasma unperturbed. Figure 5(b) shows also estimates of the polystyrene shell ablation predicted from ablation models. The models shown here are "med NGS" — a neutral gas shielding ablation model which does not include electrostatic shielding and "strong NGS" a similar model including electrostatic shielding. Overall, the models do a reasonably good job of predicting the small shell pellet ablation as shown on Fig. 5(c), but are optimistic at predicting large shell pellet ablation. This discrepancy could arise from pre-cooling (anomalous heat transport at the strongly perturbing large pellet cold front). These results show the shell has to break open before reaching the q=2 surface thus the wall thickness of the shell should be reduced to 0.1 mm on DIII-D

3. Active Feedback Control of the Runaway Beam

A robust defense against the destructive effects of the runaway electron beams requires multiple layers of protection. Should the collisional suppression mitigation methods described above fail to prevent the formation of a runaway beam, active position control can prevent the beam from rapidly colliding with the wall. Controlling the amplitude of the runaway current would provide an opportunity for slow time-scale mitigation techniques or natural decay processes to gradually terminate the runway beam without significant damage to the PFCs.

DIII-D typically utilizes a real-time EFIT (rtEFIT) equilibrium reconstruction coupled with an Isoflux control algorithm [7] for plasma boundary control. However, rtEFIT cannot produce converged equilibrium reconstructions during the rapid transients of the CQ phase. This results in a loss of Isoflux boundary control during the CQ. An alternate control algorithm that utilizes linear estimators of the plasma radial and vertical position has proven to be

robust to the transients during and immediately after the CQ. This algorithm is activated at the start of the CQ to allow for active feedback control of the runaway beam position.

The first control challenge posed by a runaway beam is to re-establish radial equilibrium immediately after the CQ. The outer poloidal coils that are primarily responsible for radial equilibrium on DIII-D, are not capable of slewing rapidly enough towards zero current to maintain radial equilibrium during the 5–10 ms CQ. Without corrective measures, the runaway beam compresses against the inner wall and, typically within 30–50 ms, terminates in a disruption without a significant loss of RE beam current. In order to avoid this compression, the inner wall poloidal coils are given saturated commands at the start of the CQ to push the plasma off the wall, while at the same time the outer coil currents are reduced as rapidly as possible. Depending upon the level of RE flattop current, the effort to push the plasma off the inner wall can result in a diverted RE beam. RE beam lifetimes up to 250 ms have been achieved using this control method. Vertical stability of the runaway beam is maintained using standard derivative control. Feedback controlled movement of the beam both above and below the midplane has been demonstrated, as shown in Fig. 6. Although the initial runaway beam is typically circular and vertically stable, vertical control is maintained even if the beam becomes elongated and diverted by the radial control. Achieving a reliable radial position control has proven to be more challenging. A successful "soft landing", wherein the RE current decays completely without any VDE or other disruption, has not yet been observed. Although the RE position can be held steady for long periods of time, every RE beam eventually terminates in a VDE. As the VDEs typically occur after significant RE current decay, often during quiescent periods well after the CQ, the instability might be due to changes in the current profile during the current decay. Avoiding such VDE's and achieving a "soft landing" will be the focus of future RE control studies.

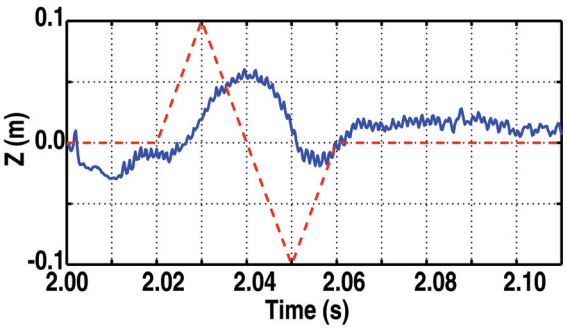

FIG. 6. Vertical position feedback control of the RE beam: vertical position of the plasma (solid) compared to the target value (dash).

In addition to position control, the ability to sustain a runaway electron current channel long enough to apply slow deconfinement techniques requires control of the RE current amplitude itself. Recent experiments in DIII-D have demonstrated that applied loop voltage V_{loop} can strongly affect the RE current amplitude, and that real-time feedback can regulate this amplitude to a desired level while the current channel persists. This capability allowed substantial increase in the duration of the RE current plateau in DIII-D from ~20 ms typical of unregulated RE currents in previous experiments up to >150 ms with regulation. Figure 7 compares discharges in which the applied V_{loop} was negative, zero, and feedback regulated to drive the RE current to 300 kA control target value. It shows a clear influence of the V_{loop} on the runaway current amplitude and that an effective feedback control on the runaway amplitude can be achieved The runaway current growth rate is approximately proportional to E-E_C, the difference between the

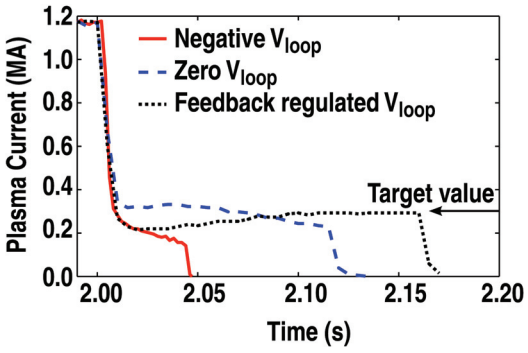

FIG. 7. RE current evolution for a different applied V_{loop}: negative (solid), zero (dashed) and feedback regulated (dotted) at I_{RE} = 300 kA.

applied electric field and the critical field, which is in turn set by the density of free and bound electrons in the background gas [1]. Further studies will examine the relation between the RE growth rate and the estimated electric field.

4. Magnetic Deconfinement of Runaway Electrons

A seed population of high-energy electrons can avalanche to convert a large fraction of the thermal plasma current to relativistic current. The dynamics of this process imply that for sufficiently high V_{loop} assumed to be produced by the plasma current decay, the final runaway current I_{RE} is related to the initial seed current I_{SEED} via $I_{RE} \sim I_{SEED}\, e^G$, where $G \approx I_P/(I_A \ln\Lambda)$, and $I_A \approx 0.02$ MA [1]. For typical DIII-D disruption experiments, the seed amplification e^G is on the order of 20–50, so that the final runaway current value depends strongly on the size of the initial seed population. Under this relatively low-gain condition, the size of the seed can provide a strong mechanism for limiting the final runaway current value by reducing the magnitude of the seed. In addition to collisional damping, reduction of either seed or avalanched runaway electron populations (and current) can be achieved through their deconfinement on open field lines [8]. This phenomenon occurs naturally during the TQ because of the violent MHD events that characterize the TQ. These instabilities typically produce a near-total loss of thermal energy on timescales much shorter than possible with cross-field transport, implying a combination of radiation and parallel transport [9]. These open field lines can also deconfine RE that precede the thermal quench (seeds) or are generated in the thermal quench. Another form of RE deconfinement due to magnetic field configuration perturbed from the target equilibrium has been demonstrated in several devices using externally applied non-axisymmetric fields [10]. Recent experiments in DIII-D have studied this effect by applying n=3 and n=1 fields using in-vessel coils. Either n=3 or n=1 fields up to 80 G at the plasma surface were applied to Ar pellet-induced disruptions in limited or diverted plasma configurations. Diverted plasmas have been observed to produce RE current channels with lower probability in DIII-D, while limited (lower elongation) equilibria produce RE current with high probability. Application of n=3 RMP fields prior to onset of the thermal quench successfully suppresses the post-disruption RE current in a significant fraction of both cases, with apparently higher effectiveness in diverted plasmas. Figure 8 summarizes the statistics for both configurations, and cumulatively. No diverted cases were observed to have visible RE current with n=3 fields applied (before the thermal quench), and a 50% reduction in incidence of post-disruption RE current was observed with limited plasmas. In contrast to the significant effectiveness of n=3 fields, no suppression was observed in either limited or diverted plasma targets with n=1 fields. Recent experiments have also studied the variation in RMP RE suppression effectiveness with time of field application. No suppression was observed if the RMP was applied after the thermal quench was complete, while the suppression statistics illustrated in Fig. 8 correspond to pre-thermal quench application of the field. One conclusion of these studies is that the RMP is incapable of deconfining RE from the mature current channel. However, the successful suppression by pre-thermal quench field application suggests that the RMP affects the seed deconfinement that occurs in the thermal quench, perhaps by altering the nature of

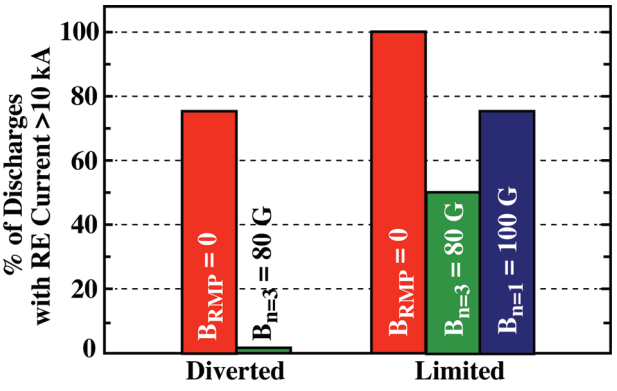

FIG. 8. Statistical distribution of successful RMP suppression of post-disruption RE current.

the MHD activity. Since heat losses during the thermal quench is dominated by open field line conduction, the degree of RE deconfinement by loss along open field lines during the thermal quench would be expected to correlate with post-thermal quench plasma impurity content since this is produced by conducted heat load to the wall. Figure 9 shows the peak RE current amplitude plotted as a function of the current quench rate for a large ensemble of Ar pellet-induced disruption diverted discharges. Four discharges with RMP suppression are also shown, corresponding to current quench rates among the highest in the dataset. The variation in RE current for the same current decay rates suggests variation in initial seed population, while the secular decline in maximum RE current with increasing initial CQ current decay rate is consistent with increased open field line transport both deconfining more effectively the initial RE seed and generating higher localized convected heat flux to the wall thus higher impurity content during the disruption. This higher impurity content increases the post-TQ resistivity thus the I_p CQ decay rate. Further analysis will be required to establish whether effectiveness of RE deconfinement on open field lines is correlated with the nature of thermal quench MHD, and if RMP fields affect these instabilities so as to enhance the deconfinement.

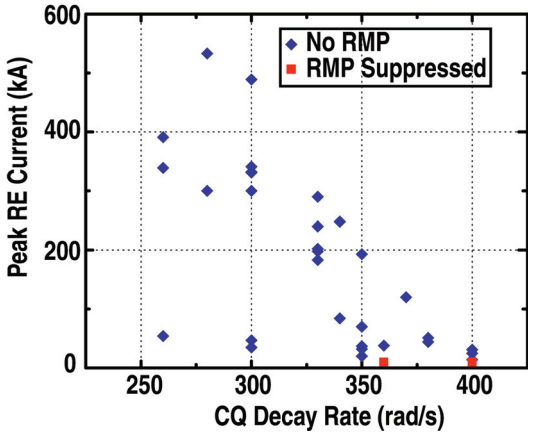

FIG. 9. Peak RE current value as a function of the CQ decay rate for the non-RMP diverted cases (diamond) and the RMP suppressed diverted case (square).

5. Conclusion

The new SPI technique has showed promising results in term of assimilation efficiency and deep penetration. The parameter scan has showed that high flow rate is critical for the efficiency of the MGI technique (explaining also the higher efficiency of SPI because of its high flow rate). The SHPI is interesting but still needs some fine tuning: the thickness of the wall has to be much thinner than previously anticipated. The low elongation limited plasma target enabled the reliable generation of significant RE currents which allowed testing mitigation techniques on an existing beam. The control of the RE position and amplitude by applied external fields has proven efficient and could allow easier mitigation by giving more time for to apply other techniques. The RMP mitigation showed some efficiency probably related to a higher MHD activity prior to the CQ.

This work was partially supported by the Oak Ridge National Laboratory managed by UT-Battelle, LLC for the US Department of Energy under contract No. DE-AC05-00OR22725 and also supported under contract DE-FG02-04ER54758.

References

[1] ROSENBLUTH, M.N., et al., Nucl. Fusion **37** (1997) 1355
[2] JAMES, A.N., et al., "Pellet Interaction with Runaway Electrons," J. Nucl. Mater., accepted for publication
[3] WESLEY, J.C., et al., "Fast Plasma Shutdowns obtained with Massive Hydrogenic, Noble and Mixed Gas Injection in DIII-D," IAEA FEC Conf., Geneva (2008) EX/7-3Rb
[4] HOLLMANN, E.M., et al., Nucl. Fusion **45** (2005) 1046
[5] COMMAUX, N., et al., Nucl. Fusion **50** (2010) 112001
[6] HOLLMANN, E.M., et al., Nucl. Fusion **48** (2008) 115007
[7] FERRON, J.R., et al., Nucl. Fusion **38** (1998) 1055
]8] IZZO, V.A., et al., this conference, THS/9-2
[9] KADOMTSEV, B.B., Plasma Phys. Control. Fusion **26** (1984) 217
[10] LEHNEN, M., et al., Phys. Rev. Lett. **100** (2008) 255003-1